A quick-scan method to assess photovoltaic rooftop potential based on aerial imagery and LiDAR

de Vries, Tim N.C.; Bronkhorst, Joris; Vermeer, Martijn; Donker, Jaap C.B.; Briels, Sven A.; Ziar, Hesan; Zeman, Miro; Isabella, Olindo

DOI
10.1016/j.solener.2020.07.035

Publication date
2020

Document Version
Accepted author manuscript

Published in
Solar Energy

Citation (APA)
de Vries, T. N. C., Bronkhorst, J., Vermeer, M., Donker, J. C. B., Briels, S. A., Ziar, H., Zeman, M., & Isabella, O. (2020). A quick-scan method to assess photovoltaic rooftop potential based on aerial imagery and LiDAR. *Solar Energy*, *209*, 96-107. https://doi.org/10.1016/j.solener.2020.07.035

A quick-scan method to assess photovoltaic rooftop potential based on aerial imagery and LiDAR

Tim N. C. de Vries, Joris Bronkhorst, Martijn Vermeer, Jaap C. B. Donker, Sven A. Briels, Hesan Ziar, Miro Zeman, and Olindo Isabella

***Abstract*—A quick-scan yield prediction method has been developed to assess rooftop photovoltaic (PV) potential. The method has three main parts. For each roof, first (i) virtual 3D roof segments were reconstructed using aerial imagery, then, (ii) PV modules were automatically fitted onto roof segments using a fitting algorithm and finally, (iii) expected annual yield was calculated. For each roof, the annual yield was calculated by three different quick yield calculation approaches. Two approaches are commercial software packages of Solar Monkey (SM) and Photovoltaic Geographical Information System (PVGIS) whereas the other one is the simplified skyline-based approach developed in photovoltaic material and devices (PVMD) group of Delft University of Technology. To validate the quick-scan method, a set of 145 roofs and 215 roof segments were chosen in urban areas in the Netherlands. For the chosen roofs, the number of fitted modules and calculated yield were compared with the actual modular layout and the measured yield of existing PV systems. Results showed a satisfactory agreement between the quick-scan yield prediction and measured annual yield per roof, with relative standard deviations of 7.2%, 9.1%, and 7.5% respectively for SM, PVGIS, and PVMD approaches. It was concluded that the obstacle-including approaches (e.g. SM and PVMD) outperformed the approaches which neglect the shading by surrounding obstacles (e.g. PVGIS). Results also showed that 3D roof segments had added value as input for the quick-scan PV yield prediction methods since the precision of yield prediction was significantly lower using only 2D land register data of buildings.**

***Index Terms*—automatic PV system design, annual energy yield, module fitting, PV potential, PV systems, quick-scan, rooftop PV, Urban PV, yield prediction.**

1. INTRODUCTION

AS humankind feels daunted by the challenge to meet their energy demand in a more sustainable and fossil-free manner, the transition to renewable energy sources such as wind and solar has begun. In 2018, global annual photovoltaic (PV) installations were surpassed 100 GW, and the total cumulative operational capacity reached over 0.5 TW [1, 2]. Even though the prices of photovoltaic systems have decreased significantly over the last decades, the adoption of PV is not increasing rapidly [3]. The mindset of society must change towards PV and PV revolution [4]. Therefore, a more societal push is necessary to help the solar PV industry grow.

Such societal push could be supported by automatic PV system design in various ways. First of all, the time required to design a PV system could be decreased considerably. Ranging from software-aided design to visual in-situ inspection (e.g. counting the number of roof tiles to have a rough estimation of roof PV potential), the actual design of a rooftop PV system may take anywhere from 10 minutes to several hours [5][6]. Because of the fierce competition in the domestic PV system market, only a small percentage of the designs are built. Much time could thus be saved on the side of the PV installation companies if the system designs on their quotations are generated automatically. An automatic PV system design can also make the sales process of PV more efficient. It would decrease the effort and time spent by cold-calling potential customers. The activity of the whole solar energy market could increase as a result of a more efficient sales process since it would increase productivity. Moreover, an advanced design algorithm could design systems with more accurate energy yields, better aesthetics or better cost-effectiveness than humans could do manually in the same amount of time. The optimal

position for modules could be calculated, minimizing the shading throughout the year. Additionally, algorithms could find alternative module configurations that would fit more modules on the same roof. For example, it could find a balance between the yield per m^2 and total yield by comparing east-west or south-directed setups according to the customer's requirements. From another point of view, by facilitating yield prediction and system design in a quick and user-friendly manner, consumers would have fewer concerns about the suitability of their rooftop for a PV system.

To fulfill this goal, a so-called *quick-scan* yield prediction method was developed. The method fully automates the design process and yield prediction of rooftop PV systems. It also enables large-scale rooftop PV potential assessments (e.g. a city or a district) by reducing the runtime as much as possible. This paper aims to introduce the quick-scan method and discuss the findings regarding the following research questions: (1) how realistic is automatic module fitting on residential rooftops? (2) how accurate is yield prediction with different quick yield calculation approaches? (3) How fast are different parts of the quick-scan method and how can this be optimized?

Section 2 gives an overview of relevant literature about the estimation of solar potential for rooftops in urban areas and briefly explains the research outline. In Section 3, the different parts of the quick-scan method are described. Section 4 shows the results of the module fitting algorithm and yield calculation approaches and discusses the simulation time. Lastly, conclusions will be drawn in Section 5, and recommendations will be presented for future work.

2. LITERATURE REVIEW AND RESEARCH OUTLINE

The potential of buildings for rooftop PV is usually determined by (i) finding the available roof area for PV modules, (ii) simulation of plane-of-array (POA) solar irradiance and, (iii) computing the annual AC energy yield of such system.

Land use, building and population densities can be used to calculate the total roof area using average conditions, and the available roof area for PV can then be found by assuming fixed utilization factors [7]. In 2010, Winginton et al. used the relation between roof surface area and population to estimate the rooftop PV power generation potential for Southeastern Ontario, US [11]. Similarly, the solar energy capacity was analyzed for different types of residential rooftops in Andalusia, Spain [12]. In 2012, Defaix et al. published the building- integrated photovoltaic (BIPV) potential for 27 European member states, starting from an average floor area per capita to find the available roof surface per country [13]. For the Indian city of Mumbai, aerial images were used to calculate values of the Building Footprint Area (BFA) ratio and the Photovoltaic- Available Roof Area (PVA), to estimate the city's PV potential [14]. An earlier Indian investigation of Delhi's PV potential was based on thumb-rules, standard assumptions and experts' opinion, due to data unavailability [15]. In 2014, Mainzer et al. analyzed the technical PV potential for each municipality in Germany, estimating the usable area and energy demand per building by statistical data [16]. In 2015, Byrne et al. calculated the net usable roof area per building type for Seoul (South Korea), including a parametric study of the module tilt and its effect on the Ground Cover Ratio (GCR) and expected PV potential of the city [17]. In 2017, Khan et al. carried out a similar study for 13 cities in the Kingdom of Saudi Arabia, and the potential electricity generation was estimated [18].

Other methodologies based on geographic information system (GIS) has increasingly used recently, particularly since GIS has become a commonly used tool [8]. If available, GIS data of the outer shapes of buildings can be used to estimate the available roof area. In 2011, the potential electricity production by rooftop PV in Israel was assessed, by using GIS data of outer building shapes and making assumptions about utilization factors [19]. Martín-Chivelet proposed an analytical expression for GCR and a step-by-step methodology for the assessment of PV potential [9]. In 2015, Freitas et al. provided a review of solar potential calculation methods for urban areas and concluded that methods should compromise between accuracy and computation time [10].

If also 3D information and/or height data is available, such as LiDAR measurements, the pitch angle, and azimuth of

roof segments can be used to determine the POA irradiance. In 2012, Brito et al. used LiDAR data to assess the photovoltaic potential in a Lisbon suburb [20]. It was concluded that for PV penetration below 10% of the total roof area, the PV potential can be well estimated by neglecting shade and considering the optimal inclination and orientation for PV, whereas, for high penetration, the potential can be estimated by considering a horizontal surface within the building footprint area. In 2011, Bergamasco et al. assessed the PV potential for rooftop-integrated PV systems using MATLAB, first by a study in the Piedmont Region [21]. Later, the MATLAB algorithm was enhanced with shadow and in-roof obstacle detection and applied to the city of Turin, processing over 60,000 buildings [22]. In 2013, Kodysh et al. combined LiDAR data and a GIS approach to estimate irradiance on different roof surfaces for Knox County, Tennessee, USA [23]. The output of the study was however solar irradiance per roof surface area since the available area for PV and electricity output were out of the scope of the research. In 2014, the rooftop PV potential of Taiwan was assessed, using GIS data for the available roof area and taking into account shading caused by other buildings [24]. There are some examples in which 3D city models are used to calculate the total roof area and expected electricity generation, such as the work of Rodriguez et al. for Ludwig- burg, Germany [25]. However, 3D city models are expensive to create or acquire, and currently unavailable for most regions in the world. Moreover, shading calculations with 3D models and ray-casting are computationally demanding and, therefore, restrict the scale for which the PV potential can be determined.

Some of the studies described above calculate the discrete amount of PV modules to be placed on the available roof area by GCR factors, however, none of them computed the actual modular layout that would fit on each roof segment. The only exception to that is a research carried out by Mainzer et al. in 2017 in which geographical building data and aerial images in combination with image recognition techniques were utilized to virtually place modules on roofs [26]. Their module fitting algorithm incrementally iterates over the usable area and fits as many PV modules as possible within each roof segment. However, it neglects a distance to be taken from the roof edge and module alignment with the edges for flat roofs.

For simulation of POA irradiance and computing the annual AC energy yield, various levels of detail could be applied in yield calculation models. For example, skyline profile (the outline of land and buildings around a PV system defined against the sky) affects the amount of solar irradiance that reaches a PV module [27]. Although shading reduces the PV module performance [28], in yield prediction approaches, the skyline profile is usually not determined for each roof, neglecting the shading caused by it. More advanced yield calculation models including non-linear effects of temperature, module technology, and inverter utilization significantly increase the runtime and fairly improves the accuracy [26]. However, when dealing with a big batch of roofs, both *accuracy* (closeness of a dataset, in this case the modelled PV yields, to the perfect prediction line on which the modeled and measured kWh/kWp values are the same) and *precision* (closeness of a dataset, in this case the modelled PV yield, to their own average kWh/kWp line) are important.

Real-life situations can lead to systematic and random errors in PV modeling. Systematic errors shift away the modeled data points from the perfect prediction (reference) while random errors cause the modeled data points to be scattered. Systematic and random errors respectively relate to accuracy and precision. For large scale studies or initial investigation (quick-scan) of a batch of rooftops, precision is as important as the accuracy. The reason is, obtaining precision is way faster than accuracy and needs less inputs and/or detailed modeling and, when a precise batch of output data for PV potential of rooftops is found, then all the results can be shifted (tuned) by a simple (and fast) correction factor to have both precise and accurate batch of output data. Therefore, the aim of this research is to develop a method that can quickly scan the PV potential of many roofs with high precision and, then, further modify it by a correction factor to have also an accurate result dataset. It is worth noting that applying one correction factor to all the yield predictions will improve several individual PV systems yield prediction while it might worsen the yield prediction of a few. However, the overall prediction for all the PV system will improve.

The method developed in this research uses 3D roof segment data, generated from aerial images and GIS data, to assess the

discrete number of PV modules to be fitted on each roof. The module fitting is tested by selecting buildings that already have PV systems on their roofs and comparing results to the number of modules that were actually placed. Also, LiDAR height data is used to account for the effects of shading by surrounding obstacles. The precision of three different yield calculation approaches is obtained using AC yield measurements of real PV systems. The developed method tries to keep the calculation time as low as possible, in order to make the algorithm usable for rooftop PV on a regional or national scale.

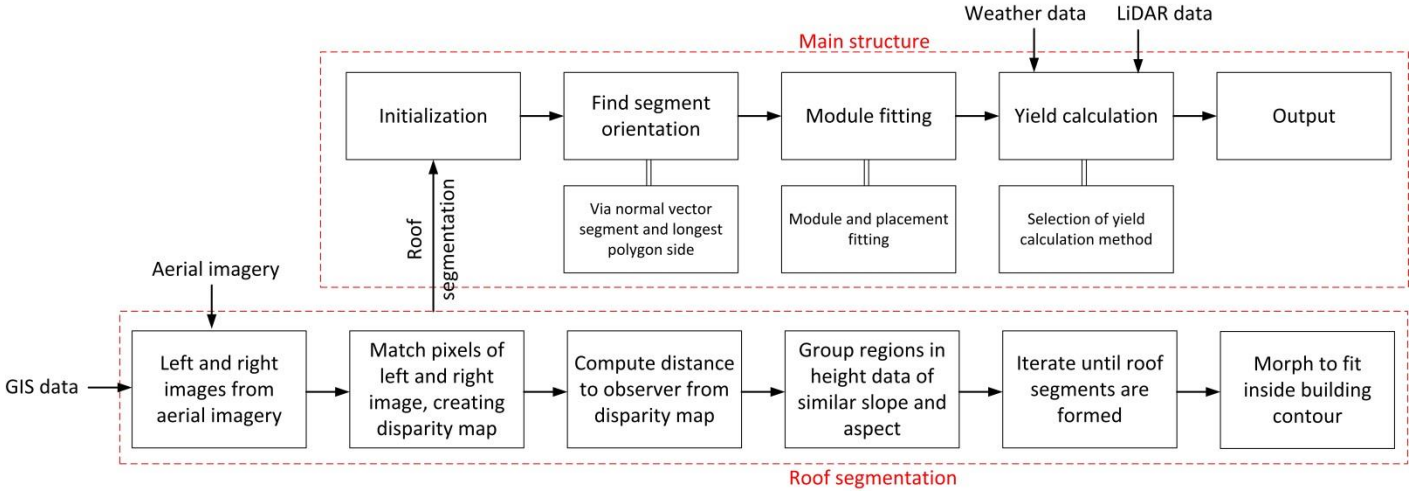

Fig. 1: The general structure of the quick-scan method. Flowchart of roof segmentation using aerial imagery feeds the quick-scan method. Weather, GIS, and LiDAR data were also used as inputs to the quick-scan method.

3. METHODS

In figure 1, general structure of the quick-scan algorithm is shown. To initialize, a set of roofs divided into 3D roof segments is fed into the algorithm. For each segment, the segment orientation is calculated, making use of two independent methods. Then module fitting is carried out, to find the maximum amount of modules that can be placed on them. For the solution accommodating most modules, yield calculation is carried out per roof segment. Finally, the output of the quick-scan algorithm will be the number of fitted modules, their expected annual AC yield in kWh and the specific annual yield kWh/kWp, each aggregated per roof or physical address. Prior to PV system installation, the widely used merit by the industry and research communities is either kWh or kWh/kWp, which give indications on how much the PV system will yield. However, after installation, to monitor the difference between the expected and the real PV yields, the merit performance ratio (PR) is used. Since the target of this research was yield assessment of the roofs, kWh and kWh/kWp were used as merits.

3.1. Roof segments extraction

In order to develop a quick-scan that works for any address, it is necessary to have information about the roofs: roof area (for PV module fitting), its slop and orientation (for yield prediction). One way is to use land register data of the buildings contours which is accessible in several countries. However, most roofs do not consist of one flat plane and have obstacles which are not detectable in buildings contours. In this research, roofs are divided into segments with different slope and orientation using stereo aerial images. The algorithm is shown in the lower part of figure 1. A roof is selected by using the building contours from land register data for the target building. A disparity map is made by matching the roof pixels of a pair of aerial images taken from a different angle (stereo-matching in GIS [29][30]). A 3D point cloud is then obtained by comparing many points on a roof, as shown by a disparity map in figure 2.

Since different segments have different orientations and pitch angles, their colors are slightly different in an aerial image. In order to split the roof into different segments, a first segmentation is carried out on the basis of color. This color filtering

creates a large number of small segments, as visible in the left part of figure 3. After this, the height data is used to unify segments with similar orientations, pitch angles and heights. These orientations and pitch angles are found by calculating the normal vectors of the planes that form the segments. The remaining segments form a 3D representation of the roof segments and potential obstacle segments like chimneys or roof windows. This process is shown in figure 3 and described in further detail in [30].

Small roof segments and segments that are on the shadow side of an aerial image are more difficult to detect. This is caused by a lack of height data points for small segments, and little contrast to find a stereo-pair of pixels in the shade. Also, the difference in color at the borders of segments is harder to detect for shaded roof segments [31].

To make the segments cover a larger part of areas within building contours and to straighten the edges of roof segments, three additional steps were applied automatically to the roof segments:

1) For neighboring roof segments which intersect in 3D, such as for hipped roofs and gable roofs, the line of intersection between the planes was determined. The roof segments are filled from both sides up to this line.
   For neighboring roof segments that do not intersect, but have a height difference, a line of intersection is drawn in the middle when looking at them in the z-direction. The roof segments are filled from both sides up to this line.
2) For the parts of roof segments that stretch to the edges of the building contour, the segment will be filled up to the edge of this land register shape.

In figure 4, a group of roof segments is shown. As it can be seen in figure 4, after applying the three aforementioned steps the edges of roof shapes are much straighter.

Fig. 2: Images (a) and (b) represent a same roof from two slightly different angles. The two stereo aerial images are used to obtain a 3D point cloud for a roof, shown in a disparity map on figure (c), obtained from [30]. Black dots shows the parts of the roof where could not be fully re-constructed by the roof segment algorithm. Since the difference in angle between the two images is known, the displacement of a point between the two images is solely dependent on the height [30].

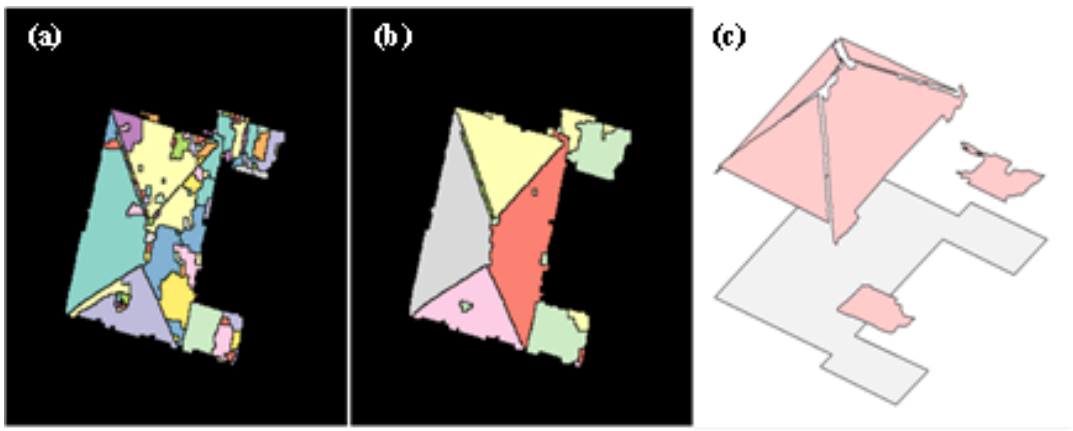

Fig. 3: Image (a) shows several small segments that are constructed based on their color in the aerial image. In image (b), to form the neat roof segments, adjacent small segments were unified based on their orientation, pitch angle, and height. In image (c), the roof segments are shown in 3D projected above the building contour, obtained from [30].

The orientation of a roof segment was determined by taking the horizontal projection of the normal vector to the segment plane. However, this orientation determination approach might cause an error for flat roofs. Therefore, an alternative approach for orientation determination was developed.

Fig. 4: Aerial image and roof segments, created before (left) and after (right) three straightening steps were applied. The small mismatch between the edges of the roofs and the segments is caused by the fact that the aerial image was not taken at exactly 90°. Since the segmentation of the roofs is dependent on the building contours, the contrast and the colors in the aerial image, sometimes segments contain flaws: (1) shaded roof segments are rarely detected. This is often a problem for low flat roofs next to taller houses. (2) sometimes existing roof segments are not detected because they were outside of the land register perimeter. This could be because of a recent house renovation or outdated land register data. Garden sheds, garages and building extensions can be overseen for this argument. (3) sometimes obstacles are detected or left out of the roof segments by the stereo-matching, either excluding from all segments or forming separate roof segments.

Throughout this research, roof segments with a slope of less than 10 degrees were categorized as flat, and segments with a higher slope were considered pitched. This boundary was chosen based on architecture and building construction industry [32], as no scientific studies were found to set this variable differently according to PV standards.

The length of each line segment was determined for the x and y coordinates, and then the longest side of the polygon within the roof segment, the longest polygon side, was chosen. For the longest polygon side, the orientation can be determined by the following equation:

$$A_{ls} = \tan^{-1}\left(\frac{x_2 - x_1}{y_2 - y_1}\right) + 180^{\circ}, \quad (1)$$

where A_{ls} stands for the azimuth of the longest side, x_i and y_i refer to the x and y coordinates the points on the roof segment. 180° is added to make the angle positive, defined clockwise starting from the North direction.

The modules alignment with the roof segment orientation is preferred since it usually fits the largest number of modules and often regarded to be more aesthetic. Figure 5 shows an example in which 33% more modules can be fitted for an aligned setup, whereas the output per module would only drop 0.5% due to the less favorable orientation (20 degrees off south, the tilt

was 13°).

Having the azimuth of one edge and knowing that most roof segments have rectangular shapes or perpendicular angles, one can obtain the azimuth of the other three edges for flat roofs:

$$B_i = A_{ls} + \sum_{i=1}^{3} i.90^{\circ}, \tag{2}$$

$$\begin{cases} A_i = B_i & B_i < 360^{\circ} \\ A_i = B_i - 360^{\circ} & B_i \geq 360^{\circ}, \end{cases} \tag{3}$$

where i= 1,2 and 3, so A_i are the three orthogonal components to A_{ls}, which are always between 0° and 360°, ensured by the constraints in equation 3. From here, the direction closest to the South (180°) will be chosen as the module orientation for all flat roof segments.

3.2. Maximum module fitting technique

A fitting algorithm was developed and implemented to place the maximum number of PV modules on top of a roof. The following input settings were chosen:

- Module dimensions of 165×99 cm^2 and the rated power of 300 Wp were chosen. The thickness of the modules is not of interest to the quick-scan.
- For flat roof segments, all modules were expected to be installed in a landscape manner with a fixed and tilt and row space (most dominant layout on flat roof).
- For pitched roof segments, the module is placed directly onto the segment. There is no row distance between modules. The module layout can be either in portrait or landscape, and both options are investigated to find the maximum module configuration. Thus, for all pitched roof segments, the fitting algorithm is carried out twice (one for portrait one for landscape).

Description of maximum module fitting technique is as follows. After defining the input settings, first, a rectangular module grid is created according to the settings specified for flat and pitched roofs. Then, the module grid, in this case with zero row distance, is shifted in the x and y directions. The step size was set to 10 cm in both directions, as recommended in [34]. Further, for every new position of the grid, the number of modules within the roof shape minus a set distance from the edge is counted. Finally, the position in which most modules are fitted gives the maximum module fitting solution. For a simple case of PV modules with zero tilt, a visual impression is given in figure 6. Details of several approaches for module fitting on roofs were discussed in [34].

By automatically defining obstacles as gaps in a roof segment, they can be avoided for module placement. The algorithm always checks if modules are intersecting obstacle segments. Roof segment are not always aligned with the x and y axes of the module grid. Therefore, a roof segment is automatically rotated around its center to match to the desired azimuth of the modules. Then the module grid is created. After this step, the roof shape and module grid are rotated back and the grid is translated in steps parallel and perpendicular to the module azimuth. For flat roofs with tilted modules, the row distance is inserted in the grid between the rows of modules. Figure 7 visualizes an example for the module fitting algorithm compared with manually fitted modules showing the possibility for different results caused by shape flaws in roof segments or in-roof obstacles.

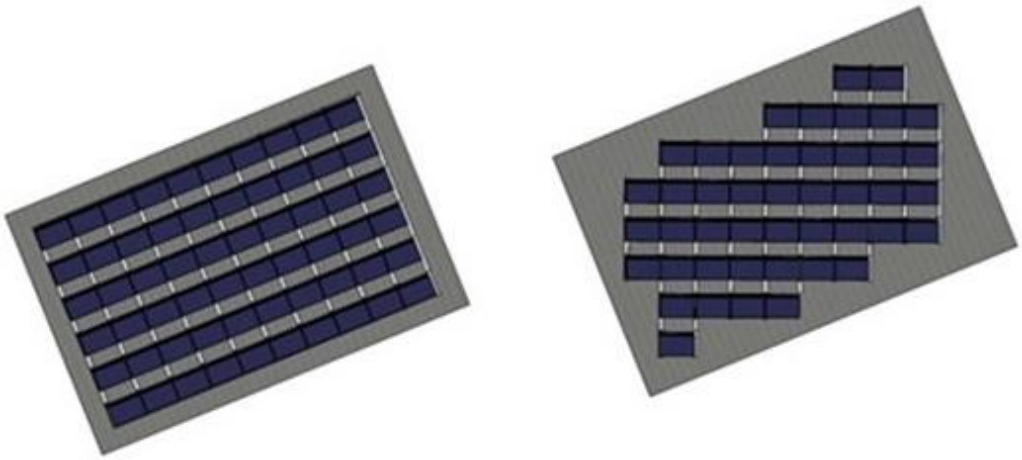

Fig. 5: Aligned with roof (left) vs due south module layouts for flat roof (right), adapted from **[33]**. It is worth noting that, from energy yield point of view, alignment of the PV modules with the roof edges is influential only for the case of the flat roofs because pitched roofs already have a fixed azimuth and tilt which PV module should comply with (mainly because of wind force and safety reasons). In general, the lower the tilt of the PV modules on a flat roof, the less influence of azimuth deviation from the true South. Besides energy yield, factors such as accessibility, cost, and aesthetics also play a role on the decision of PV modules azimuth on a flat roof.

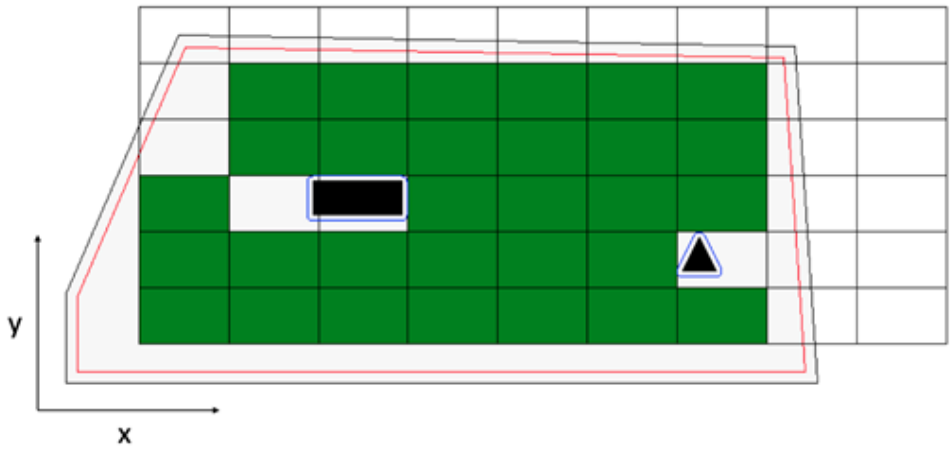

Fig. 6: A module grid (rectangular shape) is superimposed over a roof (polygonal shape) and moves around in the x and y directions, while counting the modules that fit within the roof edge minus a buffer distance without intersecting with obstacles, obtained from [34]. The figure is a screen shot of one moment of running the maximum module fitting technique.

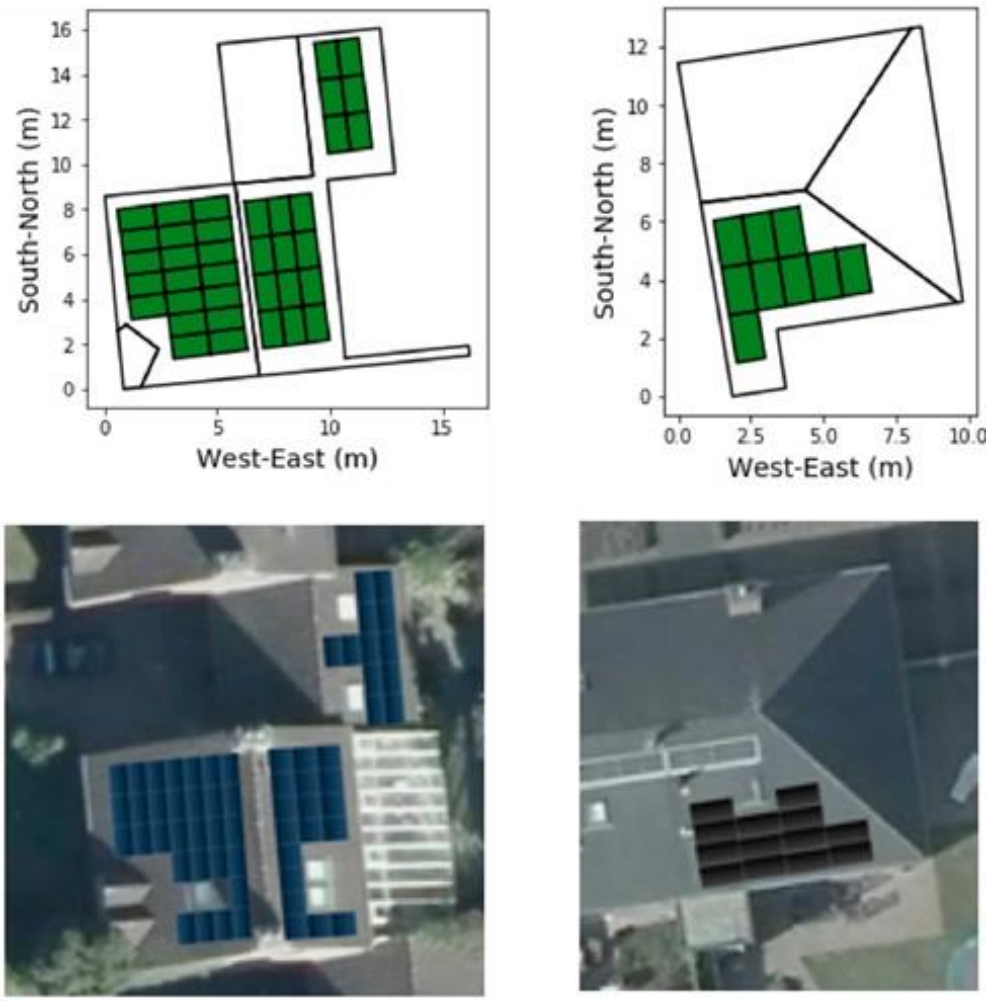

Fig. 7: Aerial images with manually placed PV modules (bottom) and corresponding visual schematics (top) of fitted modules by the algorithm, showing that module setup can yield different results due to (1) shape flaws in roof segments, and/or (2) in-roof obstacles, and/or (3) different size and orientation of the modules, and/or (4) difference in edge-distance considerations.

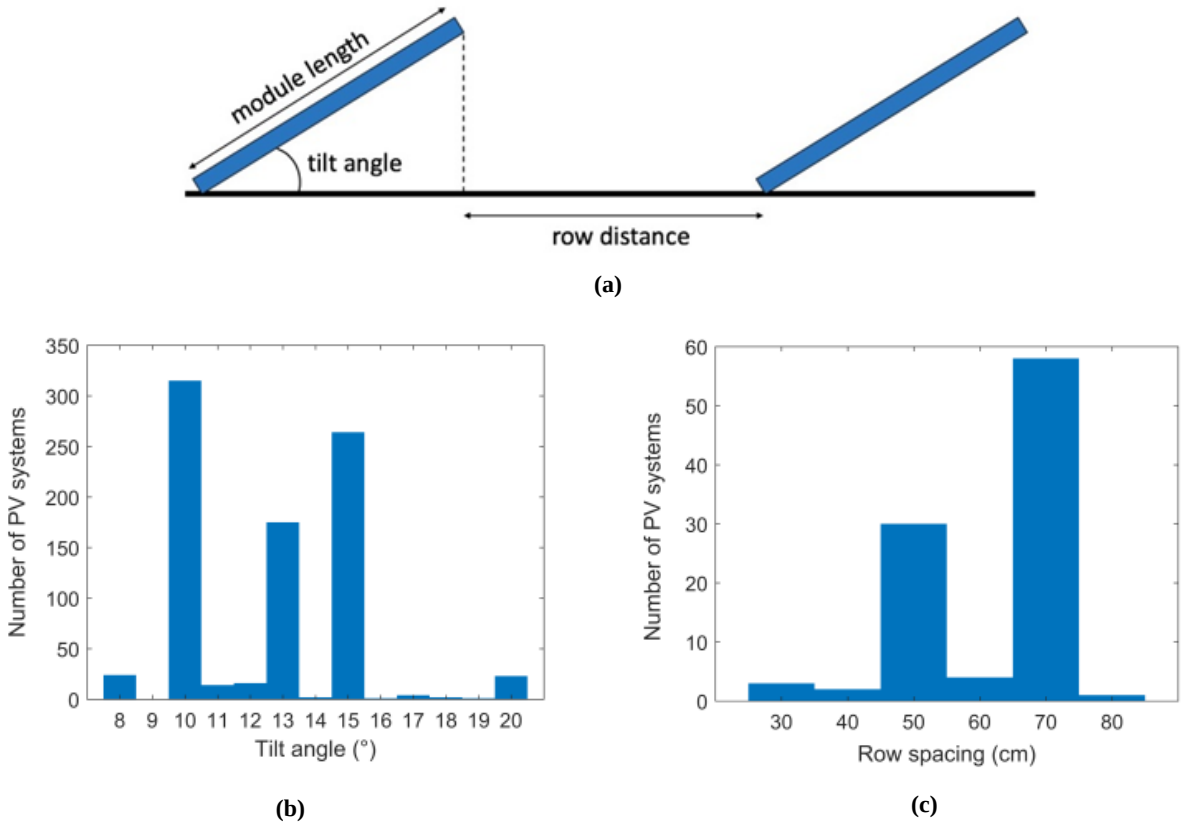

Fig. 8 (a): Schematic view of row distance between modules, (b): Counts of row spaces for installed PV systems on flat roofs which shows that the dominant row spacing in the database of Solar Monkey in the Netherlands is 70 ±5 cm, and (C): Counts of PV systems with similar tilts shows that three dominant tilt angles 10±0.5˚, 13±0.5˚ and 15±0.5˚. We chose 13 degrees as an average. It is worth noting that in an elegant PV system design, the row distance should be set based on the desired shade-free window, ground coverage ratio requirement, and the shadow length equation. In reality, however, installers use quick fixed row distance values for the Netherlands mainly driven by the two facts: (1) the tilt should be kept low because of high wind force in the Netherlands, and (2) shadow has less effect because of high share of the diffuse component in the sunlight in the Netherlands.

3.3. Yield calculation approaches

The quick-scan was designed in a modular way, so different energy yield calculation approaches can be applied and their results can be tested independently. Three yield prediction methods were investigated in this research: the first method used in this study was developed by Photovoltaic Geographical Information System (PVGIS), the second method is based on the current approach of Solar Monkey (SM), and the third method is developed by the Photovoltaic Materials and Devices (PVMD) group of Delft University of Technology [27].

In the PVGIS yield calculation method, the skyline profile is not taken into account. In PVGIS website, only the module orientation and tilt are affecting the performance. The other methods do use the skyline profile. SM approach calculates a skyline profile (or obstacle view) for every PV module that is placed on a roof. For the quick-scan, this obstacle view is only calculated for one point at the center of each roof segment. The height of this point is chosen as the highest of two height data sources. One source is the digital elevation map at the building location obtained by LiDAR, and the other source is the collection of z-coordinates of the roof segments found by stereo-matching. By taking the highest of both sources, situations are avoided where the central point is located slightly below the actual roof surface, resulting in extremely high obstacle losses. The PVMD yield prediction method is implemented according to how it was explained in [27]. PVMD approach uses two coefficients: Sky View Factor (SVF) and Sun Coverage Factor (SCF), respectively to indicate how much of the hemisphere is freely visible and the ratio

of hours that the sun is blocked with respect to the total amount of sun hours. For every climate, having the SVF and SCF, the yearly energy yield can be estimated using five fixed coefficients. The coefficients depend on the azimuth and the tilt angle of the PV module. In this research, these five coefficients were calculated for every 10° azimuth and tilt angle (and linearly interpolated for the degrees in between).

4. RESULTS

To test of the proposed method, a dataset of several buildings located in the region of Eindhoven, the Netherlands, was chosen. The chosen buildings have monitored PV systems on their roof. The roof segments are extracted as polygons, containing 3D coordinates of the edges for each roof segment. Each roof is marked with a unique building identification (id), linked to the land register data for each building in the Netherlands. Additionally, each identified roof segment is given a unique number. Besides the coordinates and id's, the segment slope (pitch angle) and azimuth (orientation in a horizontal plane) are given. The numbers of investigated roof segments for each part of the quick-scan method are shown in Table I. For the roof segments extraction, roofs were selected randomly whether they had PV module on top or not. For maximum module fitting technique, only roofs that had PV systems on top were manually selected. For annual yield prediction, only roofs with PV system that had reliable measured energy yield were manually chosen.

To check the performance of the quick-scan algorithm, the results of module fitting were compared to the actual amount of modules placed on a set of roofs with existing PV systems. Then, the results of yield calculation were compared to the measured energy yield of the PV systems in their first operational year.

TABLE I: Numbers of studied roof segments for each part of the quick-scan method.

Parts of the method	**No. of roof segments**
Roof segments extraction	520
Maximum module fitting technique	215
Yield calculation approaches	156

4.1. Input data

Extraction of 3D roof segments can be done by either LiDAR data or aerial imagery. LiDAR datasets are relatively expensive to gather compared to aerial imagery [35], usually less frequently updated, and not as widely available as stereo imagery. For the Netherlands, a countrywide LiDAR dataset, *actual hoogtebestand Nederland* (AHN), with the ground resolution of 50 cm exists and has been updated almost every seven years [36]. As an alternative to LiDAR data, a countrywide aerial stereo imagery (Stereo10) is available at a ground resolution of 10 cm for the Netherlands. Imagery is retrieved every year; mostly during winter and early spring, when the weather condition is good. The aerial imagery of geographical area considered in this paper is captured by an ultracam xp camera. Imagery was gathered from an altitude of 1600 m, taking into account variations in roll, pitch, and yaw of the camera, which is mounted to the airplane. Since aerial imagery has a resolution of 10 cm, the point-cloud retrieved from image matching has a density of 100 points/m^2. This is denser than the 6-10 points/m^2 of the AHN (LiDAR data). Therefore, in this research aerial imagery was used for roof extraction while LiDAR data was used for reconstruction of the horizon around the roofs. Besides, for the target geographical area, the data from network of weather stations in the Netherlands, known as *Koninklijk Nederlands Meteorologisch Instituut* (KNMI), was used as input for PV yield calculations [37]. Depending on the KNMI station, the availability of ambient parameters and their resolution might be different. In this research weather data with the resolution of one hour was used.

4.2. Roof segments

On average, it takes one-fourth of a second (0.257 seconds) to reconstruct the roof segments of a residential building. Within the studied set of roofs, 93% of the roof segments larger than 1 m^2 were detected.

The approach described for finding the segment orientation was tested for a set of 520 roof segments, using the orientation given in the data set as a reference. For pitched roofs, with a roof pitch higher than 10°, the deviations between the two sources of segment orientation are generally small. The absolute error was found to be within 6.3° for 95% of the pitched segments. All 28 pitched segments with an error higher than 5° were inspected manually to find the true orientation of the roof segment. Only for pitched segments with deviation values above 16° the method was found to be inaccurate. For these cases, in 7 out of 10 segments the algorithm found a wrong edge (as the closest one to the South). This was caused by segmentation errors or non-rectangular roof segment shapes.

4.3. Module fitting

First, in module fitting technique, the tilt and row distance should be set (see figure 8(a)). A tilt of 13◦ was chosen for modules because this is a common setting for mounting PV modules in the Netherlands as low module tilt reduces ballast requirements and increases the roof area utilization (see figure 8(b)). A distance of 70 cm was maintained as the horizontal distance between the projected end of a tilted module and the front side of a consecutive row (see figure 8(c)).

A visual inspection was carried out for 215 roof segments (total 145 roofs) by comparing recent aerial images with the roof segments. The segments on which PV modules placed were added to a list of manually selected roof segments. In this way, the module fitting algorithm and yield estimation approaches were tested more precisely. The following three roof groups were detected:

- (group 1) 104 segments were fully used for PV installations. The maximum number of modules was placed on these segments.
- (group 2) For 66 roof segments, almost two-thirds of the surface were used. The most common reason was that obstacles within the segment were not detected in aerial imagery. Sometimes, the building owner had no desire to use the full potential of the roof, or choose for a rectangular (aesthetic) module layout instead of fitting the maximum amount of modules.
- (group 3) For 45 roof segments, almost one-thirds of the surface were used. The most common reason was that the building owner had no desire to use his entire roof for PV. However, in twenty cases very large obstacles or a multitude of them were not detected.

Visual inspections showed that assessing the performance of the module fitting technique can be affected by individual choices of house owners. To compensate for this effect, for the second and third roof segment groups, the number of fitted modules by the algorithm was manually multiplied by 2/3 and 1/3, respectively (as manual module placement ratios). Although it was possible to divide the roofs into more than three groups (to have more accurate compensation for roof owners' choices), the three groups gave satisfactory results while saving the time.

The results of module fitting technique, shown in figures 9 and 10, reveals that the module fitting algorithm generally fits fewer modules on roofs than the real number of installed PV modules. The module placement was underestimated by 17.5% on average, with a relative standard deviation (RSD) of 46.3%. There could be multiple reasons for this under-estimation:

- Shape flaws in the roof segments mainly caused by over-segmentation (the algorithm mistakenly identifies more roof segments within a roof than what it is in reality) is the first reason. Additionally, parts of roof segments in the shade were not occasionally detected by the stereo-matching, decreasing the available area for modules to be placed.
- The categories of module placement ratios were set manually by looking at low-resolution images, which might have caused mistakes.

- The algorithm settings for module layouts could be different from reality. Smaller PV modules, lower module tilt on flat roofs and, therefore, smaller row distances might have been chosen by the installers. These options were not investigated in further detail.

An average module fitting time of 1.01 seconds per roof segment was found, with a standard deviation (SD) of 1.08s. Since the time per roof is strongly dependent on the segments within a roof, the module fitting time per roof was not analyzed further. The large standard deviation in module fitting time per segment comes from the wide variety in segment area within the data set, and the difference in module fitting time between flat and pitched segments (for pitched roof segments, the fitting algorithm is carried out twice, refer to Section 3.3). The module fitting speed was 30.4 (SD=18.2) m^2s^{-1}. The module fitting speed for pitched roofs without internal obstacle segments was 20.1 (SD=5.0) m^2s^{-1}, whereas the module fitting speed for flat roofs was 56.9 (SD=12.0) m^2s^{-1}. For flat and pitched roofs , the module fitting time per segment are shown in figure 11.

4.4. Yield calculation

After having the roofs automatically filled with PV modules, the specific annual yield is calculated for each roof segment and compared with measured data of installed PV systems. As discussed in Section 2, only the *precision* of three yield calculation approaches is evaluated. This was decided since with a large batch of roofs, the average offset in *accuracy* in yield estimation can quickly be corrected by a multiplication factor, as long as desirable precision is achieved. In this research, after running the quick-scan (panel fitting plus yield calculation) for all roof segments and obtaining the result dataset, the precision of the dataset is calculated. Then, the whole dataset is shifted by a single multiplication factor (1.0412) to be as close as possible to perfect prediction (high accuracy). Although the modelling accuracy for a few PV systems might drop, the multiplication factor improves the overall accuracy of the modelling. The results of quick-scan method for each yield prediction approach are shown in Table II. Figure 12 shows the results for the SM yield calculation approach in a scatter plot with an RSD value of 7.2%.

TABLE II: Final results of the quick-scan per yield prediction approach, all roofs with pitched segments with orientation errors above 16° were filtered out (resulting 132 roofs and 156 roof segments).

Yield prediction approach	**SM**	**PVMD**	**PVGIS**
Relative Standard Deviation	7.2%	7.5%	9.1%

It can be concluded that the SM method is marginally more precise than the PVMD method. The PVGIS method performs significantly worse, which can be explained by the fact it does not take into account the skyline profile.

The calculation times of the yield prediction were found to be 6.93s (SD=0.56s), 6.50s (SD=0.44s) and 1.31s (SD=0.21s) per roof segment for the SM, PVMD and PVGIS approaches, respectively. Since a real roof in the Netherlands has an average of about 4 roof segments, the calculation times per roof required for SM, PVMD, and PVGIS would be in the order of 28, 26 and 6 seconds, respectively. Since the calculation time per roof is very dependent on the number of roof segments taken into account, the calculation speed could be greatly increased by filtering out low-potential roof segment beforehand. A low-potential segment would not fit a significant amount of modules (e.g. less than 3) or is pitched towards the North and, therefore, generates less than 650 kWh/kWp per year. By choosing a minimum segment area of 8 m^2, and only using pitched segments with an azimuth orientation between 75 and 285 degrees (South=180°), the calculation time per roof could be halved without compromising the precision of the results. Further research can be done on the optimal boundaries for such preliminary filtering.

For all yield prediction approaches, it was observed that the RSD increased for roofs with higher levels of shading, which is caused by the fact that only one point per roof segment (middle point) was considered for obstacle detection. Additionally, shaded

segments have fewer data points that can be matched based on color recognition, such that the inaccuracy in segment orientation and pitch angle becomes larger. It was found that the three yield prediction approaches perform very similarly for roofs with an SCF below 0.25, however for roofs with a higher SCF the SM and PVMD approaches greatly outperform PVGIS because of neglecting the obstacle view by PVGIS.

For the SM yield prediction approach, the yield prediction accuracy and precision were analyzed for different sizes of roof segment. In this effort, the complication occurred that the performance could only be validated on roof level, while the yield prediction was carried out per roof segment. To overcome this, an average segment area was defined for each roof within the manual selection on which modules were placed. The average segment area per roof was a weighted average of the segment areas, by the amount of fitted modules, to reflect their contribution to the performance of the whole roof. For the full set of manually selected roof segments, the average roof segment area was 36.5 m^2. The roof segments were categorized (based on size) into three groups of less than 25 m^2 (small), between 25m^2 (medium) and 70m^2, and more than 70 m^2 (large). Figure 13 shows the results for three categories of roofs, containing small segments, medium-sized segments, and large segments. The groups represent 35, 80 and 30 roofs, respectively. The results are described below:

- A high RSD is obtained for small roof segment group. The reason could be explained by the over-segmentation of several roof segments in the stereo-matching process. An over-segmentation of a suitable roof can lead to a smaller amount of modules fitted on it and, therefore, bias the yield prediction importance of a less suitable roof segment. Additionally, smaller segments contain fewer pixels in the point cloud and ,therefore, given values for roof pitch angle and orientation are less accurate.
- Medium-sized roof segments resulted in the highest accuracy prediction and the highest percentage of performance over-prediction. This over-prediction could be caused by unidentified obstacles within the roof segments, but also by the customer choosing not to use the best-performing segment, but place modules on a slightly lower-performance one.
- The most different result is found for the large roof segments. Their performance is generally under-predicted, while the RSD is highest with 11.7%. There could be multiple reasons for this. It might be that using one obstacle view is too inaccurate for large roof segments. A large roof segment could be divided in highly shaded parts and parts that are virtually free of any shade, so one reference point in the center might not be enough for obstacle view. Apart from that, large roof segments are seldom filled with modules. More often, it was encountered that they were only used partially. In this case, the installer would select the less shaded parts for installing PV modules. These decisions could make it difficult to test the improvement of performance prediction per roof. It would require selection of the part of a roof segment where PV was installed, either by manual inspection of aerial images or by pattern recognition of the PV modules through machine learning.

Here, two techniques are proposed to deal with large roof segments more accurately:

1) When the roof is large and more than a specific amount of modules is fitted, the PV array could be divided into multiple smaller parts. A boundary could be set at, for instance 10 modules or about 3 kWp, since this can be considered as the boundary for small residential systems. For each part of the module grid, a central point could be defined and thus the yield prediction could be done more accurately. An advantage of this techniques would be that the actual positions of modules are taken into account (not the middle of the roof segment). A disadvantage is that still a new method needs to be developed to erase modules from the system design.

2) Another method could be to divide large roof segments in smaller segments. For example a roof size of 33.4 m^2 could be chosen, since this was found as the average surface area of a roof which fits 10 modules. In this way, sub-segments with low performance could be discarded, and selection on high performance segments would then be possible. Parts of the roof could be considered independently. A big disadvantage of this techniques is that the sum of smaller segments cannot fit the same amount of modules as the full larger segment.

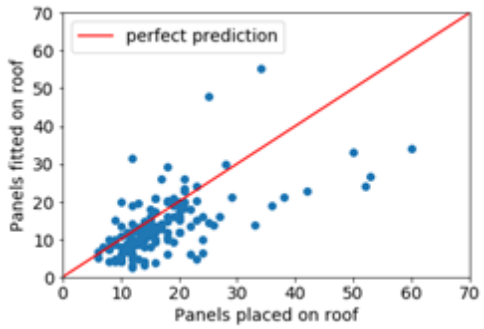

Fig. 9: Scatter plot for panel fitting on 145 roofs. Only 13.1% of the roofs are fitted with more than double the real number of installed modules.

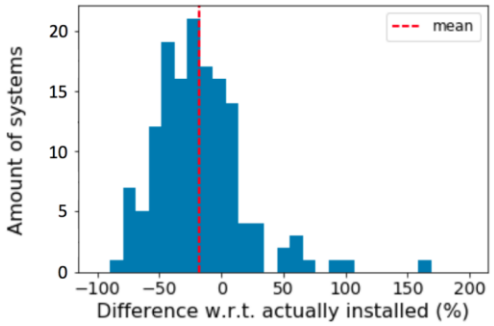

Fig. 10: Histogram for panel fitting on 145 roofs showing that for 70.3% of the roofs the amount of fitted modules was too low.

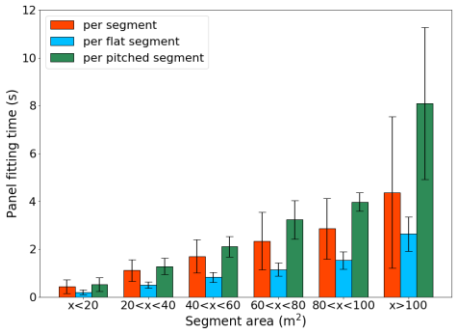

Fig. 11: Panel fitting time per segment type and area.

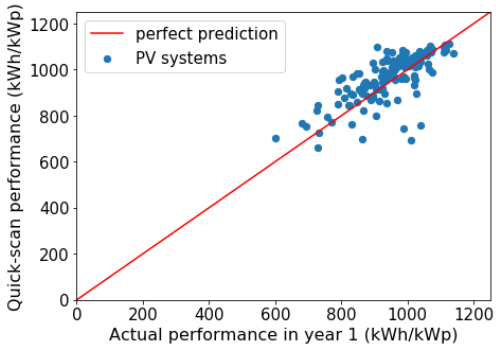

Fig. 12: Quick-scan performance prediction using SM approach for 145 roofs.

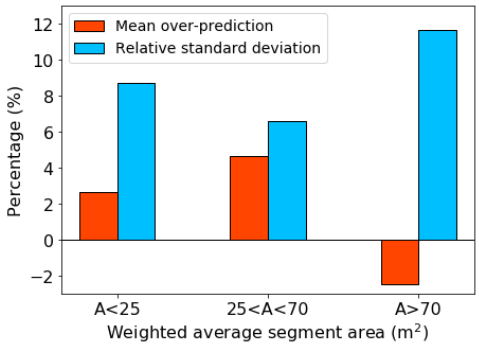

Fig. 13: Mean over-prediction and relative standard deviation of roof yield by SM approach as a function of average segment area per roof, weighted by the amount of panels fitted on it.

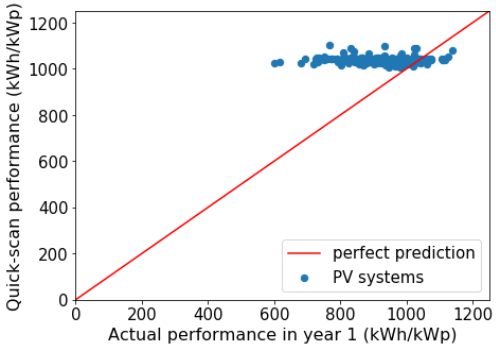

Fig. 14: Performance prediction using only land register data and no obstacle view.

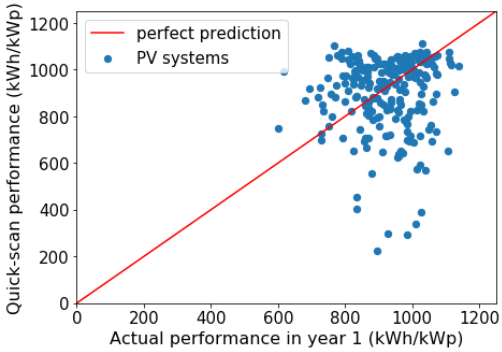

Fig. 15: Performance prediction using land register data and the obstacle view for the most central point on the roof.

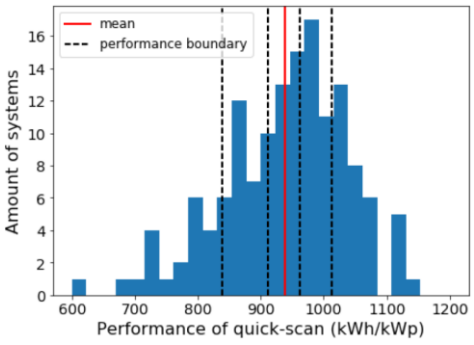

Fig. 16: Performance distribution for 236 PV systems installed in the Netherlands and being monitored.

4.5. 2D Land register data vs. 3D roof segments

To show the added value of yield prediction with 3D roof segments over using land register data only, a similar test of yield prediction was carried out using only the latter. For yield prediction with only building contours, all roofs were expected to be one-segment and flat. With this assumption, the same module settings were used as for the flat roof segments.

In figure 14 the performance prediction can be seen, using the PVGIS yield calculation method neglecting the skyline profile. The quick-scan predicts an almost constant performance, since all roofs are supposedly flat, all modules have the same tilt, and no obstacles are taken into account. The lowest value found is 1030 kWh/kWp and the highest is 1114 kWh/kWp. The only deviations in performance are caused by the slight difference in module orientation due to alignment with the roof edges and the difference in landscape horizon height as given by PVGIS. In figure 15 the same performance prediction

is carried out with the SM yield calculation method. The predicted performance shows a wide spread of results. With 20.37% relative standard deviation this form of performance estimation is not useful. Therefore, taking the obstacle view from one central point on a roof with multiple segments is not a reliable method for determining the losses due to shading.

5. DISCUSSION AND CONCLUSION

5.1. Discussion and future work

Visual comparisons reveals that still there is a room for improvement for 3D roof segment reconstruction. For example, the uncertainty in the given pitch angle is unknown, and it is unclear how often over-segmentation or under-segmentation of roof segments takes place. Another common issue was that parts with obstacles within large roof segments were not defined as gap in those segments.

For large roof segments, multiple obstacle views can be considered. Advanced geometrical methods can also be used to calculate the parallax for nearby and far obstacles. Parallax refers to the geometrical translation of shading objects over the horizon for different points on the roof. Thereby multiple obstacle views can be created from skyline profile retrieved for the center of the roof (this would be easier if the horizontal distance from obstacles to the roof is known).

The maximum module fitting algorithm could be further validated by manually choosing the same module fitting settings (layout, distance, and tilt) as used in the installed PV system. It could be investigated if the quick-scan is more accurate for flat or pitched roofs of the same size. This question remained out of the scope of the current research. It is however expected that the quick-scan would be less accurate for flat roof segments, since a larger variability was observed in the settings for module layouts (e.g. tilt angles of 0° to 20° and, therefore, very different row distances). Moreover, the boundary between flat and pitched roofs could be tuned further by inspecting many more PV systems on the roofs with the pitch angle of 5° to 15°.

The quick-scan calculation speed can be increased in various ways. The two most time- demanding steps of the calculation are the module fitting technique and creating the skyline profile from the surrounding height data. To make the module fitting technique faster, an analytical approach could be implemented for rectangular roofs, as mentioned in [34]. Fine-tuning the step size for shifting the module grid can also be investigated. Loading of height data and the calculation of obstacle views can be made faster through recommendations highlighted in [38]. Additionally, the current quick-scan code was written in a way to have many optional settings. Choosing one preferred yield prediction method or a fixed set of module settings will increase the speed, thus many *if* statements can be avoided. Moreover, making the coding more efficient, avoiding *for*-loops and a multitude of Python packages, and converting data back and forth will boost the calculation speed. Lastly, the Random Access Memory (RAM) usage can be decreased by pre-allocating arrays [39].

Roofs could also be categorized by their PV potential. Figure 16 shows the measured annual performance distribution for 236 PV systems. To quickly determine the suitability of the roofs for PV, the systems could be divided based on their performance. For example, five categories could be created with equal amounts of systems by soring the PV systems performances. This will result in four boundaries at 839.1, 911.7, 961.5 and 1012.9 kWh/kWp, respectively. Additional lower boundary can be set under which a roof is classified unsuitable. This method is easy to implement, however, in reality the PV potential is not the only variable influencing the decision of the roof owner. This method can be extended by applying a minimum amount of fitted modules to the results found by the quick-scan. If only one or two modules were fitted, it might still not be feasible to install them, since installation costs will be relatively high.

Besides kWh/kWp as the only metric for roof suitability for PV, a system design can be rated based-on performance, installation, and aesthetic aspects (as decision-making process factors). A grading system was proposed based on a fast elitist non-dominated sorting genetic algorithm for multi-objective optimization, first published by [40]. This algorithm could be implemented to categorize the PV systems that were designed on roofs by the quick-scan algorithm.

5.2. Conclusion

This research aimed to develop a method that can quickly scan the PV potential of many roofs with a high precision in a short amount of time. The paper introduced the approaches used for each stage of the quick-scan method (3D roof segment reconstruction, automatic module fitting, and yield calculation). The method was tested using a dataset of rooftop PV systems located in the Netherlands.

A simple and fast approach to determine the roof segment orientation was developed, based on the longest side of the roof segment polygon. For the set of 520 roof segments, the absolute error was found to be within 6.3° for 95% of the pitched segments. Most of the deviation were caused by the non-rectangular roof segments.

For a studied set of 145 roofs and 215 roof segments, module placement was underestimated by 17.5% on average. Multiple reasons were identified for fewer modules being fitted than actually installed: (1) over or under-segmentation, (2) different module layout, size, and spacing from roof edges, (3) different module tilt and spacing on flat roofs, and (4) modules of one PV system spread over multiple building roofs. In terms of RSD, the obstacle-including approaches (SM and PVMD) outperformed the PVGIS yield calculation. It is concluded that using only one obstacle view might cause inaccuracy for large roof segments, especially if the least shaded part of a large roof is used, this can lead to under-prediction of the PV system performance by the quick-scan method.

To demonstrate the added benefit of 3D roof segment data over 2D land register data, the module fitting and yield prediction were also carried out. The performance predictions using the SM yield prediction method were widely spread with an RSD of 20.4%, while those using the PVGIS method were relatively constant at 1070 kWh/kWp per year. The added value of 3D roof segments was thus shown.

For the quick-scan method, the required calculation times per roof for SM, PVMD, and PVGIS were around 28, 26 and 6 seconds, respectively.

Acknowledgment

The work was supported by Netherlands Enterprise Agency (RVO) via the project: PVISION with Grant No. TEUE116236. The authors gratefully thank dr. Gregory Pandraud (TU Delft) and the anonymous reviewers for the useful discussions.

REFERENCES

[1] SolarPower Europe, "Global market outlook for solar power 2019 - 2023," SolarPower Europe, Tech. Rep., Belgium, 2019.

[2] Photovoltaic Power System Programme, "2018 snapshot of global photovoltaic markets," International Energy Agency, Tech. Rep., 04 2018.

[3] E. Karakaya and P. Sriwannawit, "Barriers to the adoption of photo- voltaic systems: The state of the art," *Renewable and Sustainable Energy Reviews*, vol. 49, pp. 60–66, 2015.

[4] A. Smets, "Conference closing talk," 2017, EUPVSEC.

[5] Pramod Nepal, Remote Solar Designer, Sungevity Nederland, personal communication, October 28, 2019,

[6] R. de Proost, Managing Director, PureSolar (The Netherlands), personal communication, November 15, 2019

[7] S. Izquierdo, M. Rodrigues, and N. Fueyo, "A method for estimating the geographical distribution of the available roof surface area for large- scale photovoltaic energy-potential evaluations," *Solar Energy*, vol. 82, no. 10, pp. 929–939, 2008.

[8] J. Schallenberg-Rodríguez, "Photovoltaic techno-economical potential on roofs in regions and islands: the case of the canary islands. method- ological review and methodology proposal," *Renewable and Sustainable Energy Reviews*, vol. 20, pp. 219–239, 2013.

[9] N. Martín-Chivelet, "Photovoltaic potential and land-use estimation methodology," *Energy*, vol. 94, pp. 233–242, 2016.

[10] S. Freitas, et. al., "Modelling solar potential in the urban environment: State-of-the-art review," *Renewable and Sustainable Energy Reviews*, vol. 41, pp. 915–931, 2015.

[11] L. Wiginton, H. T. Nguyen, and J. M. Pearce, "Quantifying rooftop solar photovoltaic potential for regional renewable energy policy," *Computers, Environment and Urban Systems*, vol. 34, no. 4, pp. 345–357, 2010.

[12] J. Ordóñez, E. Jadraque, J. Alegre, and G. Martínez, "Analysis of the photovoltaic solar energy capacity of residential rooftops in andalusia (spain),"

Renewable and Sustainable Energy Reviews, vol. 14, no. 7, pp. 2122–2130, 2010.

[13] P. Defaix, et. al., "Technical potential for photovoltaics on buildings in the eu-27," *Solar Energy*, vol. 86, no. 9, pp. 2644–2653, 2012.

[14] R. Singh and R. Banerjee, "Estimation of rooftop solar photovoltaic potential of a city," *Solar Energy*, vol. 115, pp. 589–602, 2015.

[15] R. Revolution, "Unleashing delhi's solar potential," *Bridge to India in partnership with Greenpeace (New Delhi/Bangalore, India: 2013)*, 2013.

[16] K. Mainzer, et. al., "A high-resolution determination of the technical potential for residential-roof-mounted photovoltaic systems in germany," *Solar En- ergy*, vol. 105, pp. 715–731, 2014.

[17] J. Byrne, et. al., "A review of the solar city concept and methods to assess rooftop solar electric potential, with an illustrative application to the city of seoul," *Renewable and Sustainable Energy Reviews*, vol. 41, pp. 830–844, 2015.

[18] M. M. A. Khan, M. Asif, and E. Stach, "Rooftop PV potential in the residential sector of the kingdom of saudi arabia," *Buildings*, vol. 7, no. 2, p. 46, 2017.

[19] R. Vardimon, "Assessment of the potential for distributed photovoltaic electricity production in israel," *Renewable Energy*, vol. 36, no. 2, pp. 591–594, 2011.

[20] M. C. Brito, et.al., "Photovoltaic potential in a Lisbon suburb using LiDAR data," *Solar Energy*, vol. 86, no. 1, pp. 283–288, 2012.

[21] L. Bergamasco and P. Asinari, "Scalable methodology for the photo- voltaic solar energy potential assessment based on available roof surface area: Application to piedmont region (italy)," *Solar Energy*, vol. 85, no. 5, pp. 1041–1055, 2011.

[22] L. Bergamasco and P. Asinari, "Scalable methodology for the photo- voltaic solar energy potential assessment based on available roof surface area: further improvements by ortho-image analysis and application to turin (italy)," *Solar Energy*, vol. 85, no. 11, pp. 2741–2756, 2011.

[23] J. B. Kodysh, et. al., "Methodology for estimating solar potential on multiple building rooftops for photovoltaic systems," *Sustainable Cities and Society*, vol. 8, pp. 31–41, 2013.

[24] L. Ko, et. al., "Evaluation of the de- velopment potential of rooftop solar photovoltaic in taiwan," *Renewable Energy*, vol. 76, pp. 582–595, 2015.

[25] L. R. Rodr´ıguez, et. al., "Assessment of the photovoltaic potential at urban level based on 3d city models: A case study and new methodological approach," Solar Energy, vol. 146, pp. 264–275, 2017.

[26] K. Mainzer, et. al., "Assessment of rooftop photovoltaic potentials at the urban level using publicly available geodata and image recognition techniques," *Solar Energy*, vol. 155, pp. 561–573, 2017.

[27] A. Calcabrini, et. al., "A simplified skyline- based method for estimating the annual solar energy potential in urban environments," *Nature Energy*, p. 1, 2019.

[28] H. Ziar et al., "Quantification of shading tolerability for photovoltaic modules," IEEE Journal of Photovoltics., vol. 7, no. 5, pp. 1390–1399, Sep. 2017.

[29] M. Lemmens, "A survey on stereo matching techniques," *International Archives of Photogrammetry and Remote Sensing*, vol. 27, no. B8, pp. 11–23, 1988.

[30] M. Vermeer, "3D roof-models from aerial images," Master's thesis, Delft University of Technology, 2018. Available [online]: https://repository.tudelft.nl/islandora/object/uuid%3A24e59c42-b019-4fd8-a968-307eae8e4460

[31] M. Vermeer, "Large-scale efficient extraction of 3D roof segments from aerial stereo imagery," Master's thesis, Delft University of Technology, 2018.

[32] Harris, Cyril M.. "Flat roof". Harris dictionary of architecture & construction. 3rd ed. New York: McGraw-Hill, 2000. Print.

[33] Spirit Energy, "Flat Roof Solar," article on website, 2017. [Online]. Available: https://www.spiritenergy.co.uk/kb-flat-roof-solar-mounting

[34] J. Bronkhorst, "Automatic PV system design using LiDAR data shadow analysis," Master's thesis, Delft University of Technology, 2017. Available [online] : https://repository.tudelft.nl/islandora/object/uuid%3A752dfb0a-2eaf-4e3b-a0a8-ec28b3466e07

[35] Novel, Cyril, Renaud Keriven, F. Poux, and P. Graindorge. "Comparing aerial photogrammetry and 3D laser scanning methods for creating 3D models of complex objects." In Capturing Reality Forum. Bentley Systems, Salzburg, p. 15. 2015.

[36] Van der Zon, Niels. "Kwaliteitsdocument ahn2." Delft, the Netherlands (2013).

[37] https://www.knmi.nl/home

[38] G. de Koning, "Correlations and improvements of the solar monkey algorithm," Solar Monkey Data Analysis internship, Tech. Rep., 2017.

[39] S. McGarrity, "Programming patterns: Maximizing code performance by optimizing memory access," June, 2007. [Online]. Available: https://www.mathworks.com/

[40] K. Deb, et. al., "A fast elitist non- dominated sorting genetic algorithm for multi-objective optimization: NSGA-II," in *International Conference on Parallel Problem Solving From Nature*, pp. 849–858. Springer, 2000.